On the Structure and Dynamics of Ionic Liquids

Mario G. Del Pópolo and Gregory A. Voth*

Department of Chemistry and Henry Eyring Center for Theoretical Chemistry, University of Utah, 315 South 1400 East, Room 2020, Salt Lake City, Utah 84112-0850

The structure and dynamics of the ionic liquid 1-ethyl-3-methylimidazolium nitrate is studied by molecular dynamics simulations. We find long-range spatial correlations between the ions and a three-dimensional local structure that reflects the asymmetry of the cations. The main contribution to the configurational energy comes from the electrostatic interactions which leads to charge-ordering effects. Radial screening and three-dimensional distribution of charge are also analyzed. The motion of a single ion is studied via velocity and reorientational correlation functions. It is found that ions "rattle" in a long-lived cage, while the orientational structure relaxes on a time scale longer than 200 ps. As in a supercooled liquid, the mean square displacements reveal a subdiffusive dynamics. In addition, the presence of dynamic heterogeneities can be detected by analyzing the non-Gaussian behavior of the van Hove correlation function and the spatial arrangement of the most mobile ions. The short-time collective dynamics is also studied through the electric current time correlation function.

1. Introduction

Fluids composed solely of ions, such as plasmas and molten salts, have several properties which are virtually absent in liquids whose molecular components are neutral. These materials, characterized by slow decaying electrostatic interactions, have been extensively studied in the past theoretically[1] and experimentally.[2]

Recently a new class of ionic fluids, known as room temperature molten salts (RTMS) or simply ionic liquids (ILs), have prompted a significant amount of research. Like inorganic molten salts, ILs are composed solely of ions and have a high cohesive energy density, but in contrast their melting points are often less than 100 °C.[3,4] The first compounds of this class were described in 1914, but the discovery of air- and water-resistant species has motivated a resurgence of interest during the past decade.[4]

Most ILs of recent interest are based on nitrogen-rich alkyl-substituted heterocyclic cations, accompanied by different inorganic anions. By changing the anion or the lateral chains attached to the heterocyclic unit, a wide variation in properties, such as solvation, viscosity, catalytic activity, and melting point, can be obtained. In particular, the reasons for the low melting point of these materials are not clear, although an intuitive explanation is usually given: ILs consist of bulky inorganic anions paired with highly asymmetric and diffusely charged organic cations, leading to frustrated molecular packing and lower melting points.

Room temperature molten salts can show a liquid gap as large as 200 °C between the melting and decomposition temperatures, maintaining at the same time a very low vapor pressure. This fact is related to their high cohesive energy density, which is mainly given by the bare Coulombic interactions between the constituents.[5] Since their vapor pressure is nearly negligible, ILs do not generate noxious volatile residues, allowing at the

same time the efficient distillation of mixtures (solute/IL) without loss of the solvent.[6] Some species of ILs are miscible with water while others are hydrophobic, providing so new alternatives for biphasic extractions processes in which the IL can be recycled at the end of the procedure.

All the above features attracted the early attention of chemists looking for environmentally benign alternatives to the most traditional organic solvents, in turn motivating the search for novel applications in several branches of chemistry. Recently, ILs have been proposed as new high energy density materials, offering interesting possibilities as fuels and monopropellants. In particular, the nitrates of 1,3-disubstituted imidazolium cations seem to be promising models in low-thrust propulsion applications, such as orbital maneuvering and satellite station keeping.

However, despite the current level of research activity, our knowledge of most of the ILs' properties is somewhat empirical. It is clear that the spectrum of possible applications will be greatly amplified by a detailed understanding of their physicochemical behavior based on a more precise microscopic description. In this paper we present results, obtained by computer simulations, on the structural and dynamic properties of the IL 1-ethyl-3-methylimidazolium nitrate (EMIM−NO_3), whose molecular formula is presented in Figure 1. This compound shows a good compromise between the above-mentioned features and the simplicity required for extensive computational modeling.

This paper is organized as follows: In section 2 the methods used in the simulations are described, while results on the IL structure are given in section 3. The dynamic properties of the IL system are then presented in section 4, and concluding remarks are found in section 5.

2. Methods

Classical molecular dynamics (MD) simulations were performed using a potential energy function V, described by a sum of bond, angle, dihedral deformation energies, and pairwise 6−12 van der Waals interactions. In addition, Coulombic interactions between partial charges located on the atom sites

* Corresponding author. Telephone: (801) 581-7272. Fax: (801) 581-4353. E-mail:voth@chemistry.utah.edu.

Structure and Dynamics of Ionic Liquids

J. Phys. Chem. B, Vol. 108, No. 5, 2004 **1745**
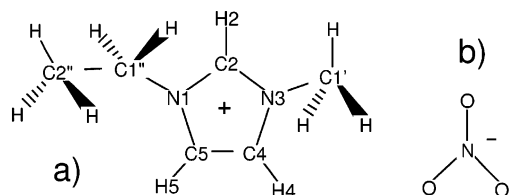
Figure 1. 1-Ethyl-3-methylimidazolium nitrate. (a) Cation (EMIM$^+$) and (b) anion (NO$_3^-$).

TABLE 1: Partial Atomic Charges for EMIM$^+$ Taken from Ref 8 and for NO$_3^-$ Taken from Ref 9^a

EMIM$^+$		NO$_3^-$	
atom	q_i/e	atom	q_i/e
N$_1$, N$_3$	−0.267	N	0.905
C$_2$	0.407	O	−0.635
C$_4$, C$_5$	0.105		
H$_2$	0.097		
H$_4$, H$_5$	0.094		
C$_{1'}$	0.124		
H in C$_{1'}$	0.064		
C$_{1''}$	0.130		
H in C$_{1''}$	0.055		
C$_{2''}$	−0.059		
H in C$_{2''}$	0.045		

^{a} See atom labels in Figure 1.

were considered. Such force fields are of a standard form, given by

$$V = \sum_{\text{bonds}} K_T(r - r_{\text{eq}})^2 + \sum_{\text{angles}} K_\theta(\theta - \theta_{\text{eq}})^2 +$$
$$\sum_{\text{dihedrals}} V_n \cos(n\phi - \gamma)] + \sum_{i=1}^{N-1} \sum_{j>1}^{N} \left[\frac{A_{ij}}{R_{ij}^{12}} + \frac{B_{ij}}{R_{ij}^6} + \frac{q_i q_j}{R_{ij}} \right] \quad (1)$$

In the case of EMIM$^+$, parameters for the stretch, bend, torsion, and dispersions were taken from the AMBER force field,[7] whereas partial charges where taken from the optimized electrostatic model developed by Hanke et al.[8] In the case of NO$_3^-$ all the parameters were taken from the paper of Baaden et al.[9] The values of all the partial atomic charges are listed in Table 1.

The system studied in this work consisted of 216 ionic pairs, or formula units (FU), with a total of 4968 atoms. Periodic boundary conditions were employed, and electrostatic interactions were calculated using the Ewald summation method. A cutoff of 12 Å for the van der Waals and the real part of the Coulombic interactions provided good convergence of the Ewald sums. The simulations were performed with the DL•POLY[10] program (version 2.13) using a time step of 0.001 ps. This time step provided a reasonable energy conservation with relative root-mean-square fluctuations in the total energy on the order of 10^{-4}. A negligible drift in total energy was observed over the duration of the simulation.

Two types of simulations were carried out. Structural and thermodynamic properties were calculated in the isobaric−isothermal (NPT) ensemble, while dynamic properties were studied in the microcanonical (NVE) ensemble. In the NPT simulations the Melchionna[11] modification of the Hoover method was used for maintaining a pressure of 1 atm and the temperature at 400 K.

Given that EMIM−NO$_3$ melts at 39 °C, a working temperature of 400 K was chosen to improve the statistical sampling. Several initially random configurations were equilibrated for 1 ns at 700 K and a pressure of 1 atm, while the temperature was
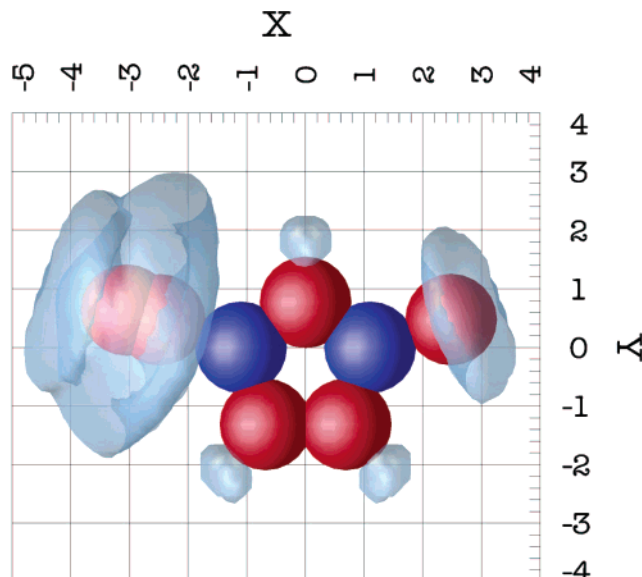
Figure 2. Isosurface of three-dimensional intramolecular configurational distribution function of EMIM$^+$ (contour level at 1.5×10^{-2} Å^{-3}). The function has been calculated with respect to a set of axes fixed in the molecule. The coordinate system is centered at the mean point of the vector going from N$_1$ to N$_3$, which defines the X-axis (see atoms labels on Figure 1). The Y-axis goes from the origin to C$_2$. The Z-axis points out of the plane of the sheet. From this plot the asymmetry of the volumes excluded by the lateral chains is clear.

subsequently lowered in two stages: 1 ns at 550 K and 1 ns at 400 K. By the end of the equilibration, total energies and volumes were monitored until the corresponding time series were stationary. Production runs then extended for an additional 500 ps.

Dynamic quantities were averaged over five independent trajectories of 500 ps each. The starting point of each simulation was the last configuration of the NPT calculations described above, although the volume of the cells was rescaled to the average volume at 400 K and 1 atm. In this way all the microcanonical simulations were performed at the same density. Production runs for the dynamical quantity calculators were preceded by 300 ps of adiabatic equilibration.

3. Liquid Structure

3.1. Internal Structure. Before discussing the equilibrium structure of the liquid, it is important to mention some features concerning the structure of anions and cations by itself. The analysis of the internal degrees of freedom showed bond length fluctuations on the order of 10^{-2} Å around equilibrium values. Bending angles fluctuated between 1° and 5°, and the angles involving hydrogen atoms on the lateral chains exhibited the largest variations. In particular, the total internal angle of the imidazolium ring was 539.3° ± 0.7°, a value which is very close to that reported by Stassen et al. for EMIM−AlCl$_4$,[12] even when the fluctuations in the present case are somewhat larger.

The equilibrium distribution of the dihedral angle C$_2$−N$_3$−C$_{1'}$−H was almost uniform, indicating a free rotation of the methyl group. In contrast, the angle C$_2$−N$_1$−C$_{1''}$−C$_{2''}$ showed two preferred conformations, corresponding to average angles of ±90°, in which the terminal CH$_3$ group of the ethyl chain is pointing outward or inward from the plane formed by the ring.

The rotation of the aliphatic chains generates two asymmetric excluded volumes on both sides of the heterocyclic unit. These volumes can be observed in Figure 2, where an isosurface of the (nonnormalized) intramolecular probability distribution

TABLE 2: Components of Configurational Energy, E_{total}, of EMIM–NO$_3$ at 400 K and 1 atm^a

E_{total}	E_{Coul}	E_{vdW}	E_{im}	RT
−209.0	−307.9	−69.8	168.7	3.32

^{a} The energy units are kJ/mol. E_{Coul} = electrostatic energy, E_{vdW} = short-range potential energy, E_{im} = intramolecular potential energy, and RT = thermal energy.
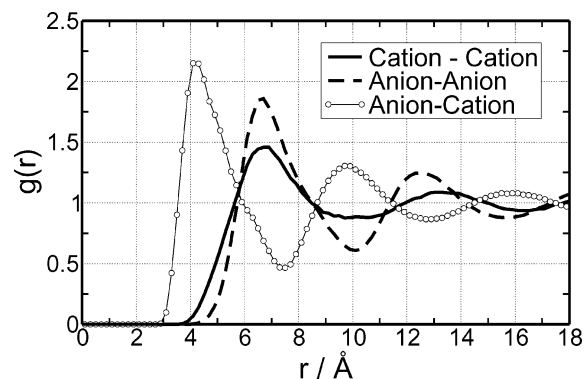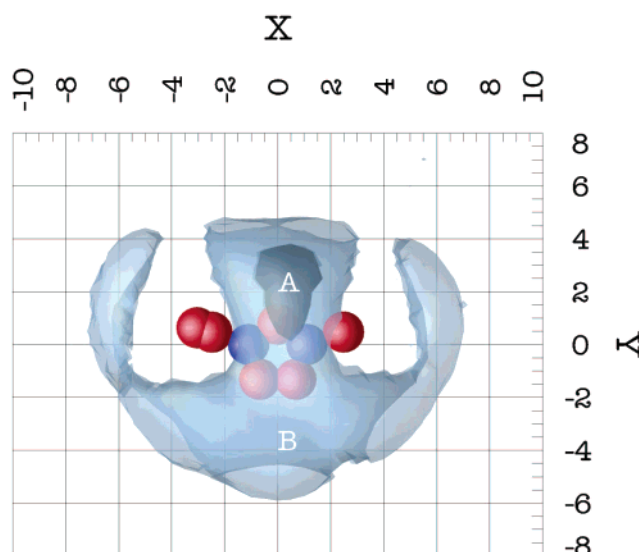

Figure 3. Radial distribution functions for the cation−cation, anion−anion, and anion−cation pairs. NPT: molecular dynamics at $T = 400$ K and $P = 1$ atm. Average density 0.004 FU/Å^3 or 1.17 g/cm^3.

Figure 4. Three-dimensional configurational probability distribution of NO$_3^-$ centers around EMIM$^+$. Two isosurfaces are shown. The dark contour surface, marked with the letter "A", has been plotted at $\rho(X,Y,Z)$ = 0.04, which is 10 times the average number density. The clear surface, marked with "B", corresponds to $\rho(X,Y,Z)$ = 0.008.

Figure 5. Three-dimensional configurational probability distribution of EMIM$^+$ centers around EMIM$^+$. The contour surface has been drawn at $\rho(X,Y,Z)$ = 0.006, which is 1.5 times the average number density of cations.

function is shown. This distribution has been calculated with respect to a right-handed coordinate system centered on the middle point of the vector going from N$_1$ to N$_3$, which also defines the X-axis. The Y-axis points from the origin to C$_2$. In addition, spheres of radius 0.75 Å have been placed on the average position of each carbon and nitrogen atom. As a result, the fluctuations of these atoms are included within the spheres.

Figure 2 outlines the shape of the object generated by the fluctuations of the intramolecular structure of the cation and gives an idea about its equilibrium structure. With the aim of showing an envelope of all the regions of high probability density, a contour surface of 1.5×10^{-2} Å^{-3} was chosen. As will be seen later, the asymmetry of the cation will manifest in the fluid structure and distribution of charges in its close vicinity.

As opposed to neutral liquids, the local structure of a molten salt is affected by a competition of two factors: packing and screening. Packing is related to the volume and shape of the molecular constituents, and can be associated with short-range interactions. Screening is due to the rearrangements of the ions in response to electric fields produced by local excesses of charge. It depends on long-range Coulombic interactions. The relative importance of these two factors is reflected by the different contributions to the configurational energy of EMIM−NO$_3$, as shown in Table 2. The main attractive contribution comes from the Coulombic energy, which is a factor of 4.4 larger than the van der Waals energy and 2 orders of magnitude larger than the thermal energy RT.

3.2. Spatial Distribution Functions. Molten salts with the above energetic behavior are also characterized by strong oscillations in the radial distribution functions and are considered as *strongly coupled* ionic systems.[15] In the present case we can distinguish three center-of-mass pair distribution functions: cation−cation $g_{cc}(r)$, cation−anion $g_{ca}(r)$, and anion−anion $g_{aa}(r)$. As can be seen in Figure 3, all of them show oscillations extending beyond 18 Å, which is approximately the half-length of the simulation box and encloses up to three coordination shells. These spatial long-range correlations has been observed in experiments[12−14,16] and simulations of other similar ILs.[5,8,17] The cation−cation distribution function, $g_{cc}(r)$, shows the broadest peaks, and a first maximum coincident with that of
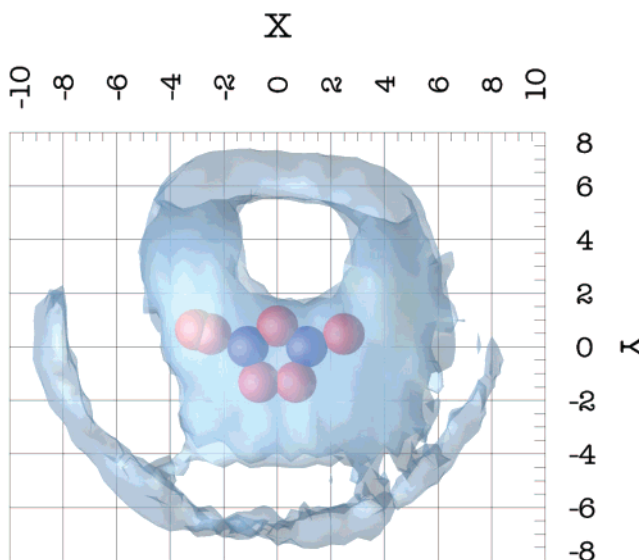
$g_{aa}(r)$ located at about 6.75 Å. The first peak of $g_{ca}(r)$ is well-defined, sharper and located at a shorter distance (4.3 Å) than in the former cases. Furthermore, the integration of $g_{cc}(r)$ and $g_{ca}(r)$ up to 7.5 Å leads to coordination numbers of 7 for NO$_3^-$ and 6 for EMIM$^+$ in the first coordination shell of the cation.

In EMIM−NO$_3$, further insight beyond isotropic radial distribution functions can be obtained by calculating the three-dimensional probability density of anions and cations centers, $\rho(X,Y,Z)$, around EMIM$^+$. Figures 4 and 5 show such three-dimensional densities for NO$_3^-$ and EMIM$^+$, respectively. In the first case two isosurfaces has been plotted. The first contour level (A), at a high probability density of $\rho(X,Y,Z)$ = 0.04, encloses two nitrates located above and below the plane of the central ring. These anions concentrate around the highly positive C$_2$−H$_2$ bond and are accounted for $g_{ca}(r)$ when integrated up to 4.5 Å. This cutoff coincides with the distance between the center of mass of the cation and the average position of the lobes A.

Structure and Dynamics of Ionic Liquids

J. Phys. Chem. B, Vol. 108, No. 5, 2004 **1747**
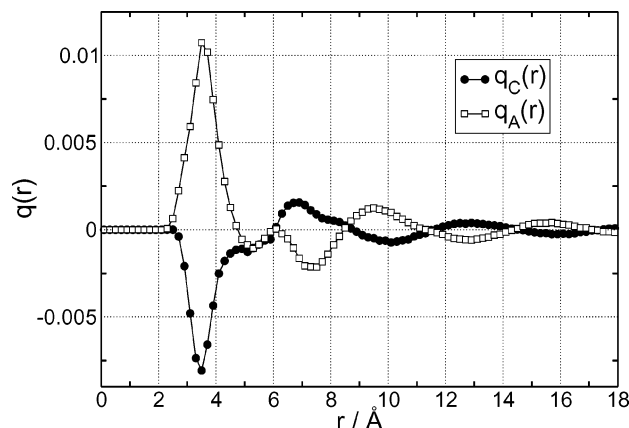
Figure 6. Radial distribution of charge around the center of mass of cations $q_C(r)$ and anions $q_A(r)$. The units of $q(r)$ are e/Å³.

Figure 7. Three-dimensional charge distribution around EMIM⁺. The yellow isosurface corresponds to $q = -0.005$ e/Å³ and the black to $q = +0.005$ e/Å³. The letters are associated with regions occupied by the anions of the first coordination shell.

The second isosurface (B) represents a lower level of probability, $\rho(X,Y,Z) = 0.008$, which is twice as large as the macroscopic density of NO_3^-. All the anions in the first coordination shell are enclosed by this isosurface, and its shape reflects the asymmetry of EMIM⁺ and the volume excluded by the lateral chains (as compared with Figure 2). By changing the probability level, one is able to find the most probable location of the seven anions in the first shell. As described above, two of them are well localized in space and their position is represented by the isosurface A. The remaining five are associated with the two lateral chains and the bonds C_4-H_4, C_4-C_5, and C_5-H_5, which are the regions where the positive charge is concentrated. The localization of these anions will be seen more clearly below when the charge distribution around cations is studied.
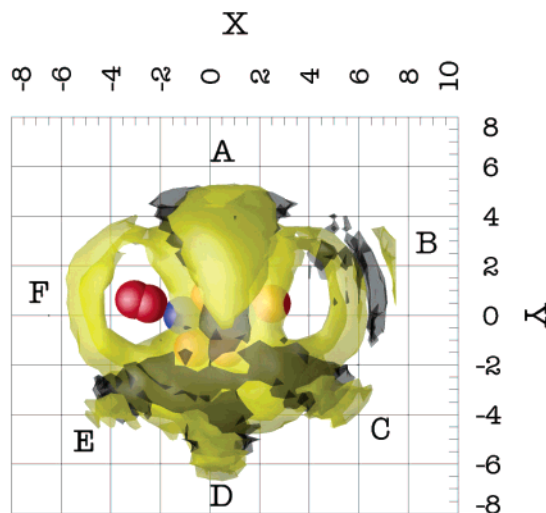
Figure 5 shows a contour surface of $\rho(X,Y,Z) = 0.006$ for the space density of EMIM⁺ centers. This value corresponds to 1.5 times the average density of the liquid and encloses all the cations located within a sphere of radius 7.5 Å. As in the case of NO_3^-, by moving the probability level we have been able to recognize two zones of high probability in the vicinity of the cation. These lobes are well localized at approximately 6.0 Å above and below the plane of the ring, and when $g_{cc}(r)$ is integrated with this cutoff, we obtain a coordination number of 2. The archlike structure running below the C_4-C_5 bond and extending up to the level of the lateral chains appears just at a relatively low density [$\rho(X,Y,Z) = 0.007$], indicating that in this region cations are less localized in space. An additional interesting feature of Figure 5 is the large void, with a size equivalent to that of the imidazolium central ring, observed in the Y-positive region above the C_2-H_2 bond.

In Figure 3, the oscillations of $g_{cc}(r)$ and $g_{aa}(r)$ are out of phase with those of $g_{ac}(r)$. This indicates a charge-ordering effect in which cations and anions are preferentially surrounded by their corresponding counterions, leading to the phenomenon of screening. The screening length, λ_D, is defined as the characteristic distance beyond which local charge neutrality is achieved, which can be quantified by the correlation length of the charge radial distribution $q(r)$.[15] For inorganic molten salts, in the strongly coupled regime, $q(r)$ is well approximated by the following functional form:

$$q(r) = \frac{A}{r}\exp(-r/\lambda_D)\sin(2\pi r/d + \phi) \qquad (2)$$

where the parameter of interest here is λ_D.[15]

Figure 6 shows the radial distributions of charges $q_c(r)$ and $q_a(r)$ around the center of mass of cations and anions, respec-

tively. These functions have been calculated from the charges supplied by every atom in the system and are somewhat different, mainly regarding the structure of the first peak, from that calculated as a linear combination of the $g(r)$'s. We have estimated λ_D from the envelope of $q(r)$, assuming eq 2 is valid for a complex molecular liquid. In a log–linear plot of $|rq(r)|$ vs r, this envelope is a straight line of slope $-1/\lambda_D$. For EMIM–NO_3 we estimated a value of $\lambda_D = 7.0$ Å for both cations and anions, indicating the effective interaction between ions decays very quickly with distance and within a length scale comparable to the location of the first maximum in $g_{cc}(r)$ and $g_{aa}(r)$.

It is important to stress that eq 2 gives just a qualitative picture about screening in a highly structured fluid of nonspherical components. In particular, the details observed between the first and second peaks of the $q(r)$'s are not reproduced by this functional form. The reported value of $\lambda_D = 7.0$ Å represents the best straight line tangent to the maxima in the $\ln|rq(r)|$ vs r representation.

Taking into account the nonsphericity of the ions, an angular dependence on λ_D can be expected. To evaluate such an effect, we calculated the three-dimensional charge distribution around EMIM⁺. Figure 7 shows two contour surfaces: the yellow one is an isosurface of $q = -0.005$ e/Å³, while the black corresponds to $q = +0.005$ e/Å³. The strong similarity with the three-dimensional configurational distribution of anions (Figure 4) indicates that practically all the charge in the first coordination shell is supplied by NO_3^-. In fact, the above positive and negative charge isosurfaces are geometrically included within the configurational isosurface B of Figure 4, and the same shape is observed.

A more distinctive feature of Figure 7 is given by a "negative–positive–negative" layering of the charge distribution, as can be observed in different regions around the cation. By disregarding the contributions of NO_3^- and EMIM⁺ to the total charge density, it can be concluded that the alternation of signs is given by the orientation of NO_3^- with respect to EMIM⁺. Oxygen in NO_3^- is negatively charged while nitrogen is positive. In the regions labeled as A, B, C, D, and E, nitrates are oriented with oxygens pointing toward the centers of positive charge in the cation. These centers are associated with the C_2-H_2 bond, the methyl group, and the bonds C_4-H_4, C_4-C_5, and C_5-H_5. In region F layers are not observed because the motion
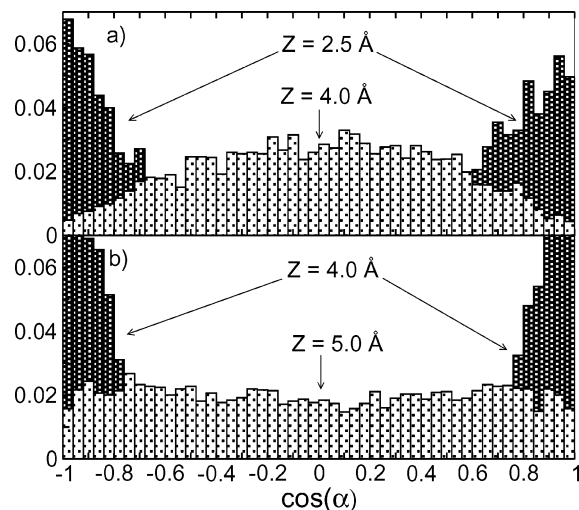
Figure 8. Static orientational correlation functions for the pairs (a) [EMIM$^+$][NO$_3^-$] and (b) [EMIM$^+$][EMIM$^+$]. α is the angle between the Z-axis of the coordinate system in the cation and a unitary vector normal to the plane of the anion. The function has been calculated within a square slice of 4 Å side, centered in the origin of the cation frame, and at different Z distances perpendicular to the EMIM$^+$ plane. A box 0.5 Å wide in the Z direction was used.

of the ethyl group randomizes the orientation of the anion. The above conclusions are additionally supported by the following observations: site−site radial distribution functions depict nitrate oxygens closer to the carbon atoms than nitrate nitrogens.

3.3. Angular Distribution Functions. Static angular correlation functions between the pairs [EMIM$^+$][NO$_3^-$] and [EMIM$^+$][EMIM$^+$] provide additional useful information. Figure 8a shows the distribution of cos(α) for the pair [EMIM$^+$][NO$_3^-$]. Here α is the angle between the Z-axis normal to the plane of the cation and a unit vector normal to the plane of the anion. The functions were calculated for the nitrates sampled from square boxes of 4 Å sides in the directions parallel to the cation ring and centered in the origin of the cation frame (0.0,0.0). A box 0.5 Å wide in the Z-direction was used, and the functions were then calculated at varying Z locations. At Z = 2.5 Å, NO$_3^-$ and EMIM$^+$ planes are preferentially oriented parallel to each other. At Z = 4.0 Å, a distance which coincides with the regions of positive charge in Figure 6 and the first maximum of $g_{ca}(r)$, the distribution of angles shows a clear maximum at $\pi/2$, indicating their planes tend to be perpendicular. Finally, for values of Z greater than 6.5 Å the distribution of angles is uniform. The same conclusions hold for sampled regions other than parallel to the cation plane except the F region. There the distribution of angles is uniform even for positions very close to the ethyl chain.

Figure 8b provides similar angular correlation information for the pair [EMIM$^+$][EMIM$^+$]. At Z = 4.0 Å, cations tend to be parallel to each other, while at all larger Z values the cations' relative orientation becomes a uniform distribution.

4. Dynamical Properties

A thorough study of the microscopic dynamics of ionic liquids is important for better understanding their chemical reactivity, rheology, electrical conductivity, and mass transfer. These properties will play a major role in applications of room temperature molten salts as alternative solvents, propellants, and conductors. Transport properties of ILs have been recently addressed in the context of liquid fragilities[19] and the design of new electrolytic conductors.[20] From the point fo view of

chemical reactivity, it has been suggested that chemical reactions are diffusion limited even for highly soluble molecules.[18] Furthermore, ILs show very long equilibration times against the absorption of gases, this observation being related to the low diffusivity of the solutes on a highly viscous medium.

4.1. Velocity Correlation Functions. One insight into the microscopic motion of the ions can be gained by the center-of-mass velocity autocorrelation functions (VACFs), resolved on both the laboratory (L) and molecular (M) frames.[21] In general, a VACF can be written as $C^L(t) = \langle \mathbf{V}^c(t)\cdot\mathbf{V}^c(0)\rangle$, where the vector $\mathbf{V}^c(t) = \sum_k m_k\mathbf{v}_k(t)/M$ is the velocity of the center of mass of the molecule and the scalar product is calculated in the usual L-frame defined by the basis vectors $\mathbf{i}_l$ ($l = x, y, z$).

One can also consider the velocity autocorrelation function, $C^M(t)$, resolved in the mobile M-frame, where each particular molecule looks fixed. This coordinate system was described at the beginning of section 3 and is spanned by the time-dependent unit vectors $\mathbf{i}_m(t)$ ($m = X, Y, Z$). For the L-frame VACF we have

$$C^L(t) = \langle \mathbf{V}^c(t)\cdot\mathbf{V}^c(0)\rangle = \sum_l \langle V^c l(t)\, V^c l(0)\rangle$$

$$= \sum_m \langle \mathbf{V}^c(t)\cdot\mathbf{i}_m(0)\, \mathbf{V}^c(0)\cdot\mathbf{i}_m(0)\rangle$$

$$= \sum_m C_m^{\,L}(t) \tag{3}$$

while for the M-frame VACF

$$C^M(t) \equiv \sum_m \langle V_m^c(t)\, V_m^c(0)\rangle$$

$$= \sum_m \langle \mathbf{V}^c(t)\cdot\mathbf{i}_m(t)\, \mathbf{V}^c(0)\cdot\mathbf{i}_m(0)\rangle$$

$$= \sum_m C_m^{\,M}(t) \tag{4}$$

In the last definition it is important to note that due to the rotation of the M-frame, at times not equal to zero, $\mathbf{i}_m(t)\cdot\mathbf{i}_{m'}(0) \neq \delta_{m,m'}$.

In parts a and b of Figure 9 normalized versions of $C^L(t)$ and $C^M(t)$ are shown for cations and anions, respectively. In both cases the VACFs are quite similar and the first zero indicates a mean collision time of approximately 0.2 ps due to the "cage" effect. Subsequently the correlations monotonically weaken within 1 ps for cations and 0.5 ps for anions, and no evidence of long-time tails is detected. This monotonic behavior can be contrasted with that of inorganic molten salts formed by ions of different size. There the smaller ion shows a marked backscattering, indicating that part of the initial momentum is returned to the central particle, while the motion of the biggest ion is mainly diffusive.[1]

One intriguing feature of the curves in Figure 9 is the strong similarity between $C^L(t)$ and $C^M(t)$, given that the last function involves the rotation of the molecular frame. To investigate this behavior, the orientational correlation functions $\Omega_m(t) = \langle \mathbf{i}_m(t)\cdot\mathbf{i}_m(0)\rangle$ were calculated for each axis of the M-frame of cations and anions. As can be observed in Figure 10, the correlation time of the rotational motion is orders of magnitude longer than the decorrelation time of the VACFs, indicating an important separation of time scales between rotational and translational motion. A similar difference of time scale is

Structure and Dynamics of Ionic Liquids

J. Phys. Chem. B, Vol. 108, No. 5, 2004 **1749**
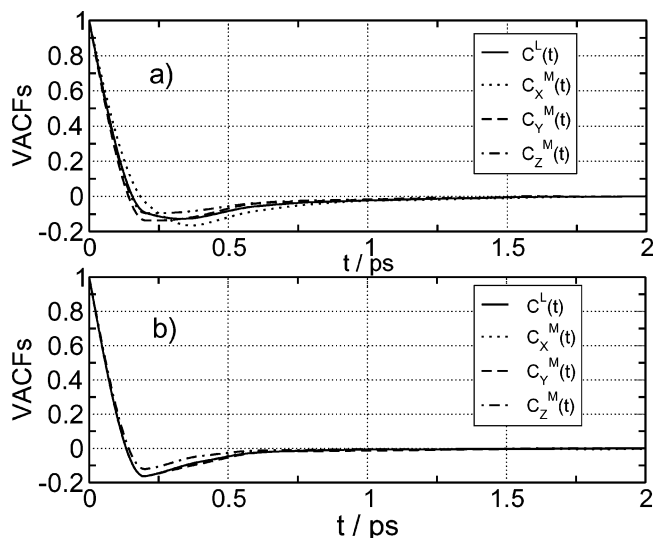
Figure 9. Velocity correlation functions (VACF) of (a) $EMIM^+$ and (b) NO_3^- at 400 K and density of 0.004 FU/Å^3. $C^L(t)$ is the VACF calculated in the laboratory frame while $C_X^M(t)$, $C_Y^M(t)$, and $C_Z^M(t)$ are the three components of the VACF projected in the molecular frame.
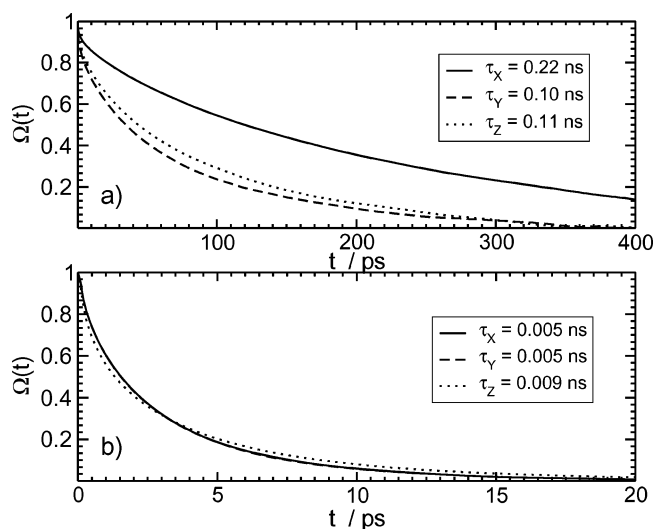

Figure 10. Orientational correlation functions $\Omega_m(t)$ for each axis of the molecular frame of (a) cations and (b) anions. The correlation times τ_m have been calculated by fitting an exponential function to $\Omega_m(t)$.

observed between the rotations of cations and anions, as shown by the relaxation times, τ_m, annotated in Figure 10. The values of τ_m have been calculated by fitting an exponential function to $\Omega_m(t)$. In the case of $EMIM^+$ (Figure 10a) the reorientation of the *X*-axis, coincident with the vector connecting the nitrogens, is a factor of 2 slower than the other two. This indicates that the lateral chains slow the rotational diffusion of the cation. Nitrate reorientation is slower for the *Z*-axis (perpendicular to its plane) but, even so, orders of magnitude faster than the reorientation of the cation.

Taking into account the slow decay of the functions $\Omega_m(t)$, the similarity between $C^L(t)$ and $C^M(t)$ is explained in the following way: anions and cations librate in a long-lived cage while the orientational structure relaxes on a much longer time scale. The coincidence of $C^L(t)$ and $C^M(t)$ follows from the fact that ions maintain the same orientation while the velocity autocorrelation functions decay to zero.

4.2. Self-Diffusion Behavior. A second way of characterizing the single-particle dynamics in a dense fluid is through the mean
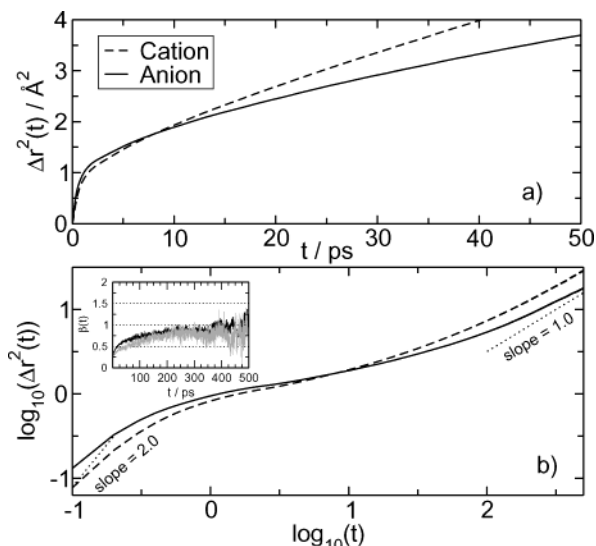
Figure 11. Upper panel (a): linear scales plot of the center-of-mass mean square displacements (MSDs) of $EMIM^+$ (dashed line) and NO_3^- (solid line). Lower panel (b): log−log plot of the MSDs using the same line styles for the different species as in the upper panel. Dotted lines of slope 1 and 2 have been included as an aid in identifying the two limit regimes: $\langle|\Delta r(t)|^2\rangle \propto t^2$ and $\langle|\Delta r(t)|^2\rangle \propto t$. Inset: $\beta(t) = d \log(\Delta r^2)/d \log(t)$ as a function of time. The black line corresponds to $EMIM^+$ and the gray to NO_3^-.

square displacement (MSD)

$$\langle\Delta|\mathbf{r}(t)|^2\rangle = \frac{1}{N}\langle\sum_{i=1}^{N}|\mathbf{r}_i^c(t) - \mathbf{r}_i^c(0)|^2\rangle \tag{5}$$

calculated from the center of mass $\mathbf{r}_i^c$ of the molecules. This function has two limiting behaviors:[1] at short times the motion of the ions is almost ballistic so that $\langle|\Delta\mathbf{r}(t)|^2\rangle \propto t^2$; at long times after the molecules have experienced many collisions $\langle|\Delta\mathbf{r}(t)|^2\rangle \propto t$. On intermediate time scales the shape of $\langle|\Delta\mathbf{r}(t)|^2\rangle$ will depend on the specific system under consideration and the thermodynamic state. In particular, plateaus have been observed in supercooled liquids before the glass transition.[22,23]

Parts a and b of Figure 11 show the MSDs at 400 K for cations and anions on linear and logarithmic scales, respectively. Looking at the linear−linear plot, one is tempted to conclude that the dynamics becomes diffusive after nearly 10 ps, as suggested from computer simulations of other similar ionic liquids.[8,17] However, Figure 11b reveals that, at least in the present case, the situation is not as simple. Three different regimes can be distinguished: first, the expected stage of inertial motion occurs on a time scale of a few femtoseconds; then, a sublinear regime extends from 1 to 400 ps for both NO_3^- and $EMIM^+$; and, finally, the linear behavior associated with normal diffusion is approached at the longest times. In the same plot lines of slope 1 and 2 have been included as an aid in identifying the two limit regimes.

The most remarkable feature of the MSDs is given by the long cage escape time of the ions during the intermediate stage. As mentioned above, this kind of behavior is typical of glass formers in the supercooled region,[22] and it can be characterized by a subdiffusive dynamics where $\langle|\Delta\mathbf{r}(t)|^2\rangle \propto t^\beta$ with $\beta < 1$. In $EMIM-NO_3$ the power law seems to be strictly satisfied in the time interval 200−350 ps. This can be observed in the inset of Figure 11b, where we show $\beta(t) = d \log(\Delta r^2)/d \log(t)$ as a function of time for both anions and cations. These curves

represent the evolution of the exponent of the power law and allows one to distinguish the crossover zones. At very short times, i.e., a few femtoseconds, β is close to 2, although this feature is not clearly observed in the inset due to the linear scale in t; subsequently, there is a slow crossover in which β increases almost linearly from 0.3 up to almost 0.9. In the time interval 200−350 ps it remains constant, and we have been able to fit $\beta = 0.78$ for NO$_3^-$ and $\beta = 0.88$ for EMIM$^+$. This subdiffusive dynamics seems remarkable since the simulations were performed at 88 K above the melting point. Finally, a value of $\beta = 1$ is achieved after 400 ps.

From the last portion of the curves of Figure 11a, and using the Einstein relation $D = \lim_{t\to\infty} \langle|\Delta\mathbf{r}(t)|^2\rangle/6t$, values of $D_a = 5.8 \times 10^{-11}$ m^2/s and $D_c = 9.6 \times 10^{-11}$ m^2/s for NO$_3^-$ and EMIM$^+$, respectively, were calculated. These values are quite smaller than the diffusion coefficients of similar molecular liquids and are in qualitative agreement with those reported in the literature for other ILs.[8,12,17]

The analysis of the mean square displacements indicates that, at least within a time scale of several hundred picoseconds, the dynamics of a single ion resembles a complex non-Markovian process instead of an uncorrelated random walk. This picture is consistent with the conclusions drawn from the velocity autocorrelation functions since, again, the motion of the ions appears correlated with the slow structural relaxation of the liquid.

4.3. Dynamically Heterogeneous Behavior. To obtain further information about the molecular dynamics in EMIM−NO$_3$, especially those concerning structural relaxation, we have calculated the self-part of the van Hove correlation function, given by

$$G_s(\mathbf{r},t) = \frac{1}{N}\Big\langle\sum_{i=1}^{N}\delta(\mathbf{r}_i^c(t) - \mathbf{r}_i^c(0) - \mathbf{r})\Big\rangle \tag{6}$$

which measures the probability that the center of mass of a molecule is at position r^c at time t given that it was at the origin, $r^c(0)$, at time 0. It is possible to show that $G_s(r,t)$ has a Gaussian form at very short times corresponding to a free particle behavior and at long time scales corresponding to the hydrodynamic limit.[1] In addition, for most liquids under normal conditions $G_s(r,t)$ keeps the Gaussian form at all the times.

Supercooled liquids depict deviations from the Gaussian form at intermediate times, associated with dynamic heterogeneities,[23−25] and these deviations can be quantified by the non-Gaussian parameter,[26] given by

$$\alpha(t) = \frac{3}{5}\frac{\langle|\Delta\mathbf{r}(t)|^4\rangle}{\langle|\Delta\mathbf{r}(t)|^2\rangle^2} - 1 \tag{7}$$

where $\Delta\mathbf{r}(t)$ is the displacement at time t with respect to the position at time 0. For a Gaussian distribution of $|\Delta\mathbf{r}(t)|$, α must be equal to 0.

Figure 12 shows the van Hove function for (a) EMIM$^+$ and (b) NO$_3^-$, as calculated from the simulations $G_s(r,t)$, and as estimated under the Gaussian approximation $G_s^0(r,t) = [3/2\pi\langle|\Delta\mathbf{r}(t)|^2\rangle]^{3/2} \exp(-3r^2/(2\langle|\Delta\mathbf{r}(t)|^2\rangle))$. The non-Gaussian parameter as a function of time is shown in the corresponding insets at the delay time t^* (marked with an arrow), in which $\alpha(t)$ reaches its maximum. The functions in the main figures have been plotted at t^*. It is seen that $\alpha(t)$ is 0 during the short period of time of ballistic motion, but after that it grows, reaching a maximum value of approximately 0.4 for cations and 0.2 for anions. The maxima occur within the time interval
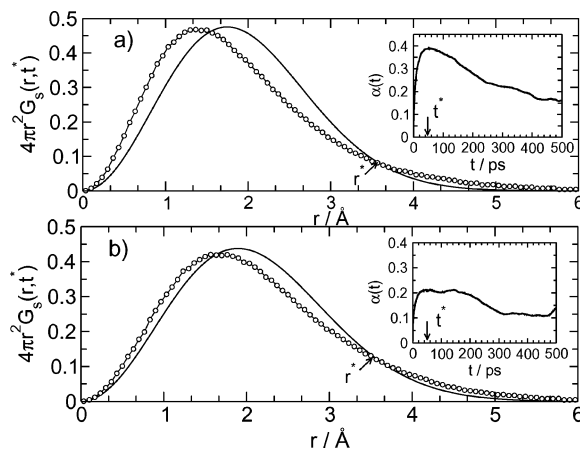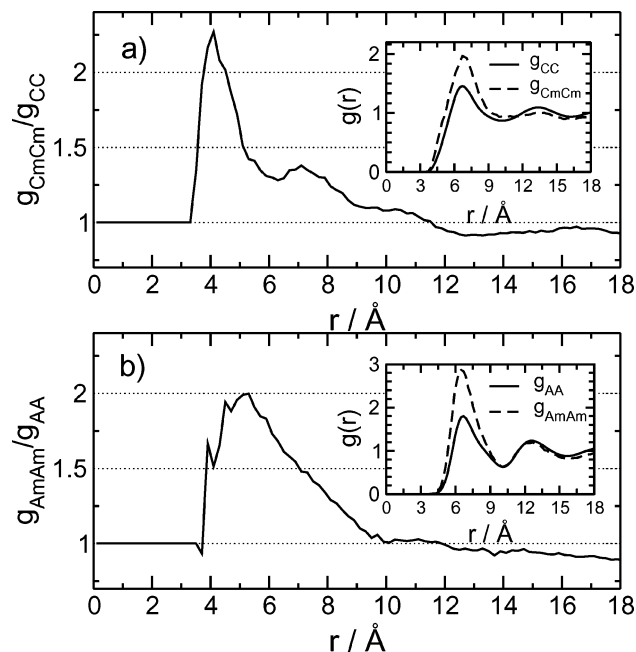

Figure 12. Main figures: van Hove correlation function $G_s(r,t)$ (line with circles) and Gaussian approximation $G_s^0(r,t)$ (solid line), for EMIM$^+$ (a) and NO$_3^-$ (b), evaluated at the delay time t^* in which the non-Gaussian parameter, $\alpha(t)$, reaches its maximum. r^* marks the crossing point of $G_s(r,t^*)$ with $G_s^0(r,t^*)$. Insets: non-Gaussian parameters $\alpha(t)$, as a function of time, for EMIM$^+$ (a) and NO$_3^-$ (b).

50−100 ps, although in the case of NO$_3^-$ it is more flat and its localization more uncertain. As mentioned before, the Gaussian form of $G_s(r,t)$ should be recovered in the long time limit and $\alpha(t)$ must decay to zero. In the present case this decay is very slow, ocurring over a time scale of 500 ps, where $\alpha(t)$ loses between 40% and 50% of its maximum value.

It has been shown for atomic[24] and molecular[25] supercooled liquids that non-Gaussian effects are related to a distribution of relaxation processes with different rates. In this case the fluid shows a spatially heterogeneous dynamics characterized by regions, or domains, of molecules of enhanced or diminished mobility. In particular, Qian et al. have shown a clear correlation between $\alpha(t)$ and the degree of heterogeneity.[25]

A complete discussion of dynamic heterogeneities in ionic liquids will be contained in ref 27. Here we shall prove their presence in EMIM−NO$_3$, and we will suggest that Kob's mechanism, based on local fluctuations in fluid structure, can explain the existence of clusters of highly mobile ions.

To study the spatial correlations between ions with similar mobility, the same procedure of Kob et al. was followed. First, the percentage of mobile particles is defined at time t^*, by integrating $G_s(r,t^*)$ from the crossing point with $G_s^0(r,t^*)$ up to an appropriate cutoff. This crossing point is marked as r^* in the main plots of Figure 12. In the present case the percentage of mobile ions at t^* involves 8% of the cations and the 9% of anions. Pair correlation functions between mobile particles of type X, $g_{X_mX_m}(r)$, can be compared with the corresponding "bulk" correlation functions, $g_{XX}(r)$, calculated from all the X particles at the same delay time t^*. The insets of Figure 13a and Figure 13b show a direct comparison of $g_{X_mX_m}(r)$ and $g_{XX}(r)$ for $X =$ EMIM$^+$ and $X =$ NO$_3^-$, respectively. At distances shorter than the first minimum of $g_{XX}(r)$, ions that traveled farther at t^* are more correlated in space than the average. This behavior is better appreciated in the main part of the figures where the ratio $g_{X_mX_m}(r)/g_{XX}(r)$ is shown. At least for distances less than approximately 11 Å, the above ratio is always greater than unity, indicating that "mobile" ions are not randomly distributed over the simulation cell but form well-defined clusters. These clusters have a kinetic nature, in the sense that ions which are "fast" at a given time become "slow" at a later time and vice versa.

Structure and Dynamics of Ionic Liquids

J. Phys. Chem. B, Vol. 108, No. 5, 2004 **1751**

Figure 13. Main figures: ratio $g_{X_mX_m}(r)/g_{XX}(r)$ for (a) X = cations and (b) X = anions at T = 400 K. Insets: direct comparison of $g_{X_mX_m}(r)$ and $g_{XX}(r)$. The pair correlation function between the most mobile particles, $g_{XX}(r)$, involves, for cations, 8% of the ions and, for anions, 9%.

By studying a binary Lennard-Jones mixture, Kob et al.[24] proposed a simple mechanism leading to dynamic heterogeneities. In this case local equilibrium fluctuations in the composition produce regions of defective packing, resulting in a higher local potential energy and increased mobility. Furthermore, Qian et al. have shown similar correlations in molecular liquids.[25] In the case of molten salts, the above mechanism could operate considering the net repulsive interaction between equally charged ions belonging to the same cluster.

From a technical point of view, local changes in the composition of ionic fluids can be difficult to detect using center-of-mass radial distribution functions. For EMIM−NO₃ the pair correlation function between "bulk" cations and mobile anions, $g_{CA_m}(r)$, was calculated and compared with the function $g_{CA}(r)$ shown in Figure 3. They are almost identical at all distances, indicating that non strong segregation of charge takes place.

However, the behavior described in the above paragraph does not mean that fluctuations in composition are absent in the present system. As was shown in section 3, charge ordering, resulting from a competition between packing and local electroneutrality, characterizes the structure of EMIM−NO₃. In addition, Coulombic energy represents the main contribution to the total configurational energy. Under such circumstances structural variations will likely involve subtle rearrangements of the ions without strong deviations from local charge neutrality. It is then possible to envision configurations in which, for example, mobile cations are grouped together, but at the same time they keep an equal number of counterions as regular "bulk" cations. In such a case counterions can be rearranged in space without altering the radial distribution of distances to the center of mass of the cation.

4.4. Electrical Conductivity. Information about the collective dynamics of the liquid can be further obtained by studying the different contributions to the electric-current autocorrelation
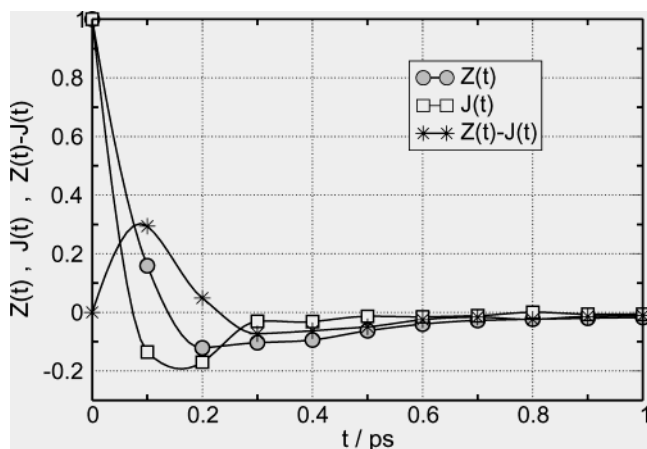
Figure 14. Total velocity autocorrelation function $Z(t)$, electric current correlation function $J(t)$, and the difference between these two functions, $-\Delta(t)$. Taking into account that $Z(0) = J(0)$, $Z(t)$ and $J(t)$ have been normalized to unity at $t = 0$.

function,

$$
\begin{aligned}
J(t) &= \sum_{i=1}^{N}\sum_{j=1}^{N}\langle z_i z_j \mathbf{V}_i^c(t)\cdot\mathbf{V}_j^c(0)\rangle \\
&= Z(t) + \sum_{i=1}^{N}\sum_{j\neq i}^{N}\langle z_i z_j \mathbf{V}_i^c(t)\cdot\mathbf{V}_j^c(0)\rangle \\
&= Z(t) + \Delta(t) \qquad (8)
\end{aligned}
$$

where z is the ionic charge and in the second and third lines self and cross terms have been shown separately.

The factor $\Delta(t)$ in the above equation measures the deviation from the ideal Nernst−Einstein behavior and provides information about the collective dynamics, given that values different from zero originate from cross-correlations in the motion of the molecules.[28] In particular, negative values of $\Delta(t)$ can be attributed to the pairing of oppositely charged ions, while positive ones indicate that the correlation between the velocities of similar ions is stronger than that between ions of different signs.

The importance of cross-correlations in EMIM−NO₃ can be assessed from Figure 14. There is shown the normalized total velocity self-correlation function $Z(t)$, which is the sum of all the self-terms in eq 8, the normalized electric current correlation function $-J(t)$, and the difference between both, $-\Delta(t)$. The difference is more important at short times, where it reaches a maximum at 0.1 ps and decays very quickly as t increases. Its positive value at short times indicates that short-lived anion−cation pairs tend to diffuse together. Under such circumstances the motion of the aggregates contributes to the mass transport but not to the electric current. However, it must be emphasized that, on the basis of the observed velocity correlations, these ionic associations are unstable and decay within a few fractions of a picosecond.

5. Conclusions

In this paper the structure and dynamics of the ionic liquid 1-ethyl-3-methylimidazolium nitrate (EMIM−NO₃) was studied by molecular dynamics simulations. The structure of the fluid is characterized by long-range space correlations between the ions and a three-dimensional distribution that reflects the asymmetry of the cations. The principal contribution to the configurational energy comes from the long-range Coulombic

interactions, and this results in charge-ordering effects. An screening length of 7 Å indicates a fast decaying effective interaction between the ions. In addition, three-dimensional charge distributions around cations show the localization of NO_3^- in different regions of the first coordination shell. The fluid structure shows a high degree of local order reminiscent of a pseudolattice of charges of alternating signs.

Velocity correlation functions calculated in both the laboratory and molecular frames, together with rotational time correlation functions, show that ions "rattle" in a long-lived cage while the orientational structure relaxes at times longer than 200 ps. As in a supercooled liquid, the mean square displacements show an intermediate subdiffusive regime for several hundred pico-seconds. In addition, the non-Gaussian behavior of the van Hove correlation function correlates well with the presence of dynamic heterogeneities. These are also detected by analyzing the spatial correlations between the most mobile ions of the system (about 8% of cations and 9% of anions) that form well-defined clusters. The short-time collective dynamics indicates the presence of short-lived anion−cation pairs.

References and Notes

(1) Hansen, J.-P.; McDonald, I. R. *The Theory of Simple Liquids*; Academic Press: New York, 1986.

(2) Bockris, J. O.; Reddy, A. K. N.; Gamboa-Aldeco, M. *Modern Electrochemistry: Ionics*; Plenum: New York, 1998.

(3) Welton, T. *Chem. Rev.* **1999**, *99*, 2071.

(4) Wilkes, J. *Green Chem.* **2002**, *4*, 73.

(5) Shah, J.; Brennecke, J.; Maginn, E. *Green Chem.* **2002**, *4*, 112.

(6) Rogers, R. D.; Seddon, K. R.; Volkov, S. *Green Industrial Applications of Ionic Liquids*; NATO Science Series; Kluwer Academic Publishers: Dordrecht, 2002.

(7) Cornell, W. D.; Cieplak, P.; Bayly, C. I.; Gould, I. R.; Merz, K. M. J.; Ferguson, D. M.; Spellmeyer, D. C.; Fox, T.; Caldwell, J. W.; Kollman, P. A. *J. Am. Chem. Soc.* **1995**, *117*, 5179.

(8) Hanke, C. G.; Price, S. L.; Lynden-Bell, R. M. *Mol. Phys.* **2001**, *99*, 801.

(9) Baaden, M.; Burgard, M.; Wipff, G. *J. Phys. Chem. B* **2001**, *105*, 11131.

(10) Smith, W.; Forester, T. R. *The DL_POLY Molecular Simulation Package;* http://www.dl.ac.uk/TCSC/Software/DL_POLY/main.html, 1999.

(11) Melchionna, P.; Ciccoti, G.; Holian, B. L. *Mol. Phys.* **1993**, *78*, 533.

(12) de Andrade, J.; Boes, E.; Stassen, H. *J. Phys. Chem. B* **2002**, *106*, 3546.

(13) Takahashi, S.; Suzuya, K.; Kohara, S.; Koura, N.; Curtiss, L. A.; Saboungi, M. L. *Z. Phys. Chem.* **1999**, *209*, 209.

(14) Hardacre, C.; McMath, S.; Nieuwenhuyzen, M.; Bowron, D. T.; Soper, A. K. *J. Phys.: Condens. Matter* **2003**, *15*, S159.

(15) Keblinski, P.; Eggebrecht, J.; Wolf, D.; Phillpot, S. R. *J. Chem. Phys.* **2000**, *113*, 282.

(16) Hardacre, C.; Holbrey, J. D.; McMath, S. E. J.; Bowron, D. T.; Soper, A. K. *J. Chem. Phys.* **2003**, *118*, 273.

(17) Margulis, C.; Stern, H.; Berne, B. *J. Phys. Chem. B* **2002**, *106*, 12017.

(18) Anthony, J. L.; Maginn, E. J.; Brennecke, J. F. *J. Phys. Chem. B* **2002**, *106*, 7315.

(19) Xu, W.; Cooper, E. I.; Angell, C. A. *J. Phys. Chem. B* **2003**, *107*, 6170.

(20) Xu, W.; Angell, C. A. *Science* **2003**, *302*, 422.

(21) Frattini, R.; Ricci, M. A.; Ruocco, G.; Sampoli, M. *J. Chem. Phys.* **1990**, *92*, 2540.

(22) Qian, J.; Hentschke, R.; Heuer, A. *J. Chem. Phys.* **1999**, *110*, 4514.

(23) Gembremichael, Y.; Schroder, T. B.; Starr, F. W.; Glotzer, S. C. *Phys. Rev. E* **2001**, *64*, 1.

(24) Kob, W.; Donati, C.; Plimpton, S. J.; Poole, P. H.; Glotzer, S. C. *Phys. Rev. Lett.* **1997**, *79*, 2827.

(25) Qian, J.; Hentschke, R.; Heuer, A. *J. Chem. Phys.* **1999**, *111*, 10177.

(26) Rahman, A. *Phys. Rev.* **1964**, *136*, A405.

(27) Del Pópolo, M. G.; Voth, G. A. To be published.

(28) Hansen, J. P.; McDonald, I. R. *Phys. Rev A* **1975**, *11*, 2111.